Selective detection of tricyclazole by optical technique using thiomalic acid–modified Au and Ag nanoparticle mixtures

Selective detection of tricyclazole by optical technique using thiomalic acid—modified Au and Ag nanoparticle mixtures

Yu-Shu Pan [a], Tsunghsueh Wu [b], Cho-Chun Hu [c], Tai-Chia Chiu [c], Chen-Hao Yeh [d], Yang-Wei Lin [a,*]

[a] Department of Chemistry, National Changhua University of Education, 1 Jin-De Road, Changhua City, 50007, Taiwan
[b] Department of Chemistry, University of Wisconsin-Platteville, 1 University Plaza, Platteville, WI, 53818-3099, USA
[c] Department of Chemistry, National Taitung University, 369 Sec. 2 University Road, Taitung, 950309, Taiwan
[d] Department of Materials Science and Engineering, Feng Chia University, 100, Wenhwa Road, Taichung City, 40724, Taiwan

Abstract

This study proposes the use of thiomalic acid—modified Au and Ag nanoparticle mixtures (TMA-Au/AgNP mixes) for the selective detection of tricyclazole. Upon the addition of tricyclazole, the color of TMA-Au/AgNP mixes solution changes from orange-red to lavender (red-shift). According to the density-functional theory calculations, tricyclazole-induced aggregation of TMA-Au/AgNP mixes through electron donor—acceptor interactions was proved. The sensitivity and selectivity of the proposed method are affected by the amount of TMA, volume ratio of TMA-AuNPs to TMA-AgNPs, pH value, and buffer concentration. The ratio of absorbance (A_{654}/A_{520}) of TMA-Au/AgNP mixes solution is proportional to the concentration of tricyclazole over the range 0.1—0.5 ppm with a linear correlation ($R^2 = 0.948$). Moreover, the limit of detection was estimated at 0.028 ppm. The practicality of TMA-Au/AgNP mixes was validated for the determination of tricyclazole concentration in real samples (spiked recovery was 97.5%—105.2%), demonstrating its advantages of simplicity, selectivity, and sensitivity.

Keywords: Aggregation, Electron donor—acceptor interactions, Pesticides, TMA-AuNPs, TMA-AgNPs

1. Introduction

With the continuous increase in population in the world, the demands for food and energy have increased. To satisfy the increased food demand, farmers worldwide use pesticides to manage crop diseases and increase crop yields. Pesticides are used to control weeds, pests, and rodents and prevent them from causing damage to agricultural and forestry crops and products. They are also used to promote crop growth by altering plant physiology and encouraging the development of beneficial insects. However, the overuse of pesticides can have severe consequences for both the environment and people. Contaminated air, water, and soil cause the contamination of fruits and vegetables, thereby increasing the likelihood of illness and poisoning upon absorption in the human body.

Tricyclazole, which is a triazole benzothiazole used to treat rice blast fungus, is a protective fungicide [1—4]. It can negatively affect the growth and function of the liver upon absorption [5]. Therefore, the detection of such harmful pesticides is crucial [6]. The WHO has also classified it as a dangerous pesticide [7—9]. Taiwan's Food and Drug Administration has stipulated pertinent guidelines for the acceptance of up to 3.0 ppm residues of tricyclazole. Pesticides are currently detected using a variety of methods [10,11]. The three most common analytical techniques are high-performance liquid chromatography [12—15], tandem mass spectrometry [16—19], and gas chromatography-mass spectrometry [20—22]. However, because of the lengthy,

intricate sample processing and expensive equipment, these techniques require skilled workers for operation.

Nanomaterials exhibit unique properties such as relatively large surface area of the volume, increased reactivity and stability during chemical processes, and enhanced mechanical strength. They are thus used in the fields of physics, chemistry, and biology for cosmetic, electrical, catalysis, and other applications [23−25]. Nanomaterials are extensively used in the fields of food and medicine [26−28]. For example, 5-sulfo anthranilic acid dithiocarbamate-functionalized silver nanoparticles (SAADTC-AgNPs) have been proposed as a colorimetric probe for tricyclaozle detection in rice samples [29]. Tricyclaozle causes SAADTC-AgNPs to aggregate (λ_{max} 400 nm shifts to 550 nm) through interactions between electron donors (tricyclaozle) and acceptors (SAADTC). Under optimum conditions, the linear range for the detection of tricyclazole is 0.189−18.9 ppm (R^2 = 0.998). The proposed SAADTC-AgNPs probe had a limit of detection (LOD) of 0.034 ppm at a signal to noise ratio (S/N) of 3.0. Furthermore, a spike recovery of 82%−85% has been demonstrated in rice samples. However, SAADTC derivatives are prepared through interactions between CS_2 and 5-sulfo anthranilic acid. Fluorescein-functionalized AgNPs (F-AgNPs) were proposed by Chiu's group as a colorimetric probe for tricyclaozle detection in rice samples [30]. This sensing mechanism was based on the interaction between tricyclazole and F-AgNPs that resulted in aggregation. The linear curve for tricyclazole detection indicated a detection range of 0.06−1.0 ppm (R^2 = 0.9994). The proposed probe also provided an LOD of 0.051 ppm at S/N of 3.0. For rice samples, the suggested colorimetric method demonstrated acceptable selectivity and satisfactory recovery (94.6%−103.0%). Compared with AgNPs, gold nanoparticles (AuNPs) exhibit higher absorption coefficient and stability [24,25]. In this study, we assumed that when tricyclazole molecules interact with recognition molecules modified on the AuNPs surface, the AuNPs crosslink and aggregate to form a new surface plasmon resonance (SPR) absorption peak. The aggregation induces a red shift in the SPR absorption peak, and a color change of the solution can be observed with the naked eye. Thus far, no study has reported the use of AgNPs and AuNPs mixtures as a colorimetric probe for detecting tricyclazole in real samples.

In this study, a colorimetric detection of tricyclaozle was proposed using thiomalic acid-modified AuNP and AgNP mixtures (TMA-Au/AgNP mixes). TMA, also known as mercaptosuccinic acid, has two carboxyl groups and one thiol group and can be used as a stabilizer for the preparation of metal nanomaterials. TMA is self-assembled on the surfaces of AuNPs and AgNPs, thereby improving their sensitivity toward tricyclaozle and their stability in aqueous solutions. The quantity of TMA, volume ratio of TMA-AuNPs to TMA-AgNPs, pH and buffer concentration were evaluated in terms of their effects on the sensitivity of the proposed method. Density-functional theory calculations were used to prove the sensing mechanism.

2. Experiment

2.1. Chemicals

All chemicals ($AgNO_3$, sodium citrate, $NaBH_4$, Thiomalic acid, $HAuCl_4 \cdot 3H_2O$, $C_4H_{11}NO_3$, Tris, HCl, cabendazim, dimethoate, trichlorfon, dichlorvos, chlorothalonil chlorpyrifos, clothianidin, glufosinate-ammonium, methomyl, 2, 4-D, propanil, glyphosate, dicofol, carbaryl, thiodicarb, acetamiprid, kresoxim-methyl, cratap, carbofuran, pencycuron, sodium diethylcarbamothioyl sulfanide, profenfos, imidacloprid, bifenthrin, and thiram) were purchased from Sigma Aldrich (St. Louis, MO, USA) and were either of analytical grade or of the greatest purity. In each experiment, Milli-Q ultrapure water was used.

2.2. Preparation of TMA-AuNPs, TMA-AgNPs, and TMA-Au/AgNP mixes

Ultrapure water (20 mL), silver nitrate solution (50 μL, 100 mM), sodium citrate solution (50 μL, 100 mM), and sodium borohydride solution (6 mL, 5 mM) were successively added to a beaker with continuous stirring. Thiomalic acid (100 μL, 0.01 mM) was then added to the beaker along with the other ingredients and stirred constantly for 1 h at 27 °C to obtain TMA-AgNPs. Tetrachloroauric acid solution (15 mL, 1 mM) and sodium citrate solution (2 mL, 38.8 mM) were heated and stirred until boiling in a double-necked flask. The solution was stirred for 15 min after being cooled to room temperature. Thiomalic acid (100 μL, 0.01 mM) was then added, and the mixture was stirred for 1 h at room temperature to obtain TMA-AuNPs. To obtain TMA-Au/AgNPs mixes, different volume ratios of TMA-AgNPs and TMA-AuNPs solutions were placed in a 50-mL sample vial for 10 min of ultrasonic mixing.

2.3. Characterization

Using a UV−Vis spectrometer, the absorption spectra of the TMA-Au/AgNPs mixes were measured in the absence and presence of pesticides (Evolution 200; Thermo Fisher, Waltham, MA, USA). Then, the TMA-Au/AgNPs mixes in the absence and presence of pesticides were characterized using transmission electron microscope (TEM, JEOL-1200EX II, Tokyo, Japan) and scanning electron microscope (SEM, JSM-6510, Tokyo, Japan). The compositions of the produced nanostructures were verified through energy dispersive spectrometry (EDS) mapping (Oxford Instruments, Abingdon, UK). A Fourier-transform infrared (FT-IR) spectrophotometer (Agilent Cary 600, Agilent Technologies, Santa Clara, CA, USA) and confocal micro-Raman system (Thermo Fisher, Waltham, MA, USA) were used to record the infrared and Raman spectra of the TMA-Au/AgNPs mixes in the absence and presence of pesticides, respectively. Using a dynamic light scattering method, the hydrodynamic diameter and zeta potential of the TMA-Au/AgNPs mixes were measured in the presence and absence of pesticides (ELSZ-2000Z, Otsuka Electronic Korea Co., Ltd., Seongnam-si, Gyeonggi-do, Republic of Korea).

2.4. Sensing process

Ultrapure water was used to generate a tricyclazole stock solution (100 ppm), which was later diluted to 1−5 ppm with ultrapure water. Separate aliquots of tricyclazole solutions (200 μL each) were added to a solution containing 100 mM Tris−HCl buffer (pH 7.0, 200 μL), 1 mL TMA-Au/AgNPs mixes, and 600 μL ultrapure water, thereby yielding final volumes of 2 mL for tricyclazole detection. The mixtures were divided into 96-well microtiter plates after equilibrating for 10 min. A Synergy H1 Hybrid Multi-Mode Microplate Reader (Agilent Technologies, Santa Clara, CA, USA) was then used to record the absorption spectra of the mixtures. These observations were recorded in triplicate for the preparation of three samples.

2.5. Extraction of tricyclazole from the real samples

Tricyclazole (200 μL, 2−4 ppm) was added to tap water (600 μL) procured from National Changhua University of Education. The mixtures were then centrifuged for 25 min at 5000 rpm and filtered through a 0.22-μm membrane. Prior to tricyclazole detection, an 800-μL membrane-treated water sample was added to a Tris−HCl buffer solution (pH 7.0, 200 μL, 100 mM) and TMA-Ag/AuNPs (1 mL). After 10 min of equilibration, the absorption spectra of the mixes were recorded using the Synergy H1 Hybrid Multi-Mode Microplate Reader. For the juice samples, tricyclazole (200 μL, 2−4 ppm) was added to apple juice (600 μL) purchased from the fruit store. After centrifugation and filtering, the pretreated juice sample was added to the Tris−HCl buffer solution (pH 7.0, 200 μL, 100 mM) and TMA-Ag/AuNPs (1 mL). After equilibration for 10 min, the absorption spectra of the mixes were recorded using the Synergy H1 Hybrid Multi-Mode Microplate Reader. Tricyclazole (200 μL, 2−4 ppm) was added to rice (25 g) purchased from a local shop. Then, the rice was soaked in 50 mL of methanol for 12 h. Then, tricyclazole was extracted by heating a mantle at 70 °C for 6 h. The solution was concentrated to 600 μL. The resulting solution was added to the Tris−HCl buffer solution (pH 7.0, 200 μL, 100 mM) and TMA-Ag/AuNPs (1 mL). The absorption spectra of the mixtures were then recorded using the Synergy H1 Hybrid Multi-Mode Microplate Reader after equilibration for 10 min.

2.6. Computational methods

All periodic DFT calculations were performed using the Vienna ab initio simulation package (VASP) [31,32]. The generalized gradient approximation (GGA) with the functional proposed by Perdew, Burke, and Enzerhof (PBE) exchange-correlation functional was used together with a plane-wave basis set with a kinetic cutoff energy of 400 eV [33]. The electron ion−core interactions were described by the projector augmented wave (PAW) method [34]. The dispersion energy correction was considered using the DFT-D3 method by Grimme et al. [35,36].

In the present work, the convergence threshold was set to 10^{-5} eV for electronic optimization, and the force convergence was set to 0.02 eV/Å for structural optimization. In the bulk Ag and Au systems, the Brillion zone was sampled using (12×12×12) Monkhorst−Pack k-points mesh, in which the optimized lattice constants of bulk Ag and Au were 4.13 Å and 4.16 Å, respectively, being in good agreements well with the experimental data [37,38]. The Au (111) and Ag (111) surfaces were considered using the p (5 × 5) supercell with three molecular layer models. The Brillouin zone integrations for the Au (111) and Ag (111) surfaces was performed using the (3 × 3 × 1) Monkhorst−Pack k-points for all structural relaxations. The adsorption energy (E_{ads}) of adsorbate was defined as the following equation:

$$E_{ads} = E_{Total} - E_{sur} - E_{Molecule}$$

where E_{Total} is the total energy of the Tricyclazole on the TMA/M(111) surfaces (M = Au, Ag), E_{sur} is the energy of the TMA/M(111) surfaces and $E_{Molecule}$ is the total energy of the Tricyclazole. Among, the TMA/M(111) surface model was carried out using the thiolate anion form ($C_4H_5O_4S^-$) of the TMA to bind on the M(111) surfaces (M = Au, Ag). In addition, Bader charge analysis was adopted to calculate the net atomic charges between the adsorbates and the TMA/M(111) surfaces [39].

3. Results and discussion

3.1. Characterization of TMA-Au/AgNP mixes by using spectroscopic techniques

UV−Vis spectroscopy, FT-IR, and DLS were used to characterize the generated TMA-Au/AgNP mixes. A distinctive SPR band of the bare Au/AgNP mixes was detected at 519 nm, as displayed in Fig. S1a [https://www.jfda-online.com/cgi/viewcontent.cgi?filename=0&article=3450&context=journal&type=additional], and the color of the solution was orange-red (Inset in Fig. S1a [https://www.jfda-online.com/cgi/viewcontent.cgi?filename=0&article=3450&context=journal&type=additional]). The SPR band of the TMA-Au/AgNP mixes was slightly shifted to 520 nm, indicating TMA assembly on the AuNP and AgNP surfaces. We obtained the FT-IR spectra of TMA and TMA-Au/AgNP mixes to demonstrate TMA molecule attachment on the AuNP and AgNP surfaces (Fig. S1b [https://www.jfda-online.com/cgi/viewcontent.cgi?filename=0&article=3450&context=journal&type=additional]). The pure TMA molecule exhibited peaks at 1695, 2564, and 3435 cm^{-1} corresponding to the stretching vibrations of the C=O, SH, and OH groups in TMA, as displayed in Fig. S1b [https://www.jfda-online.com/cgi/viewcontent.cgi?filename=0&article=3450&context=journal&type=additional] (black). The TMA-Au/AgNP mixes exhibited peaks at 1385, 1588, 1706, and 3450 cm^{-1}, corresponding to the symmetric (antisymmetric) stretching vibrations of the COO$^-$, C=O, and OH groups, respectively, as illustrated in Fig. S1b [https://www.jfda-online.com/cgi/viewcontent.cgi?filename=0&article=3450&context=journal&type=additional] (red). When compared to the pure TMA molecule, the FT-IR spectrum of the TMA-Au/AgNP mixes did not reveal the stretching vibration of the SH group. This supports the formation of a covalent bond between TMA and the surfaces of AuNP and AgNP through Au(Ag)−S linkage.

The effects of pH levels, NaCl concentrations, and storage duration on absorbance at 520 nm were tested to determine the stability of TMA-Au/AgNP mixes (Fig. S2 [https://www.jfda-online.com/cgi/viewcontent.cgi?filename=0&article=3450&context=journal&type=additional]). TMA-Au/AgNP mixes were considerably stable at pH levels 5.0−9.0. At NaCl concentrations ranging from 0 to 25 mM, the absorbance at 520 nm was almost constant. Furthermore, no changes were found throughout the first 30 days. Thus, the TMA-Au/AgNP mixes were relatively stable.

3.2. Size and morphology confirmation through SEM, DLS and TEM

The SEM and EDS mapping images of the TMA-Au/AgNP mixes are displayed in Fig. 1a. The TMA-Au/AgNP mixes exhibited a spherical shape. Signals corresponding to S, Ag, and Au elements were also observed in the EDS mapping; this indicated that S, Ag, and Au elements coexist in TMA-Au/AgNP mixes. According to EDS spectrum, the atomic contents of S, Ag, and Au in the prepared TMA-Au/AgNP mixes were 0.01%, 0.08%, and 0.71%, respectively.

The TEM images of the TMA-Au/AgNP mixes are displayed in Fig. 1b. The particles of the TMA-Au/AgNP mixes were well dispersed. The TEM images depict the small size of TMA-AgNPs mixed with TMA-AuNPs. Fig. 1b indicated that the average size of the TMA-Au/AgNP mixes in the absence of tricyclazole was 25.9 ± 4.7 nm. In addition, The hydrodynamic diameters of bare Au/AgNP and TMA-Au/AgNP mixes were 29.5 ± 6.2 and 33.7 ± 7.7 nm, respectively, as depicted in Fig. 1c. The assembly of the TMA molecule on the AuNP and AgNP surfaces slightly altered the hydrodynamic diameters of the bare Au/AgNP mixes. The attachment of the TMA molecules to the surfaces of the AuNP and AgNP increased the size of the TMA-Au/AgNP mixes. Fig. 1d depicts the zeta potentials of bare Au/AgNP and TMA-Au/AgNP mixes of −51.8 ± 1.3 and −42.8 ± 1.3 mV, respectively. The zeta potential of the TMA-Au/AgNP mixes decreased because of the substitution of citrate ions (3 COO$^-$ groups) to TMA molecules (2 COO$^-$ groups) on the AuNP and AgNP surface.

3.3. TMA-Au/AgNP mixes−based colorimetric detection of tricyclazole

We used TMA-Au/AgNP mixes as an optical probe for sensing tricyclazole and tested their colorimetric sensing capacity toward tricyclazole. Tricyclazole is an unclassified pesticide; however,
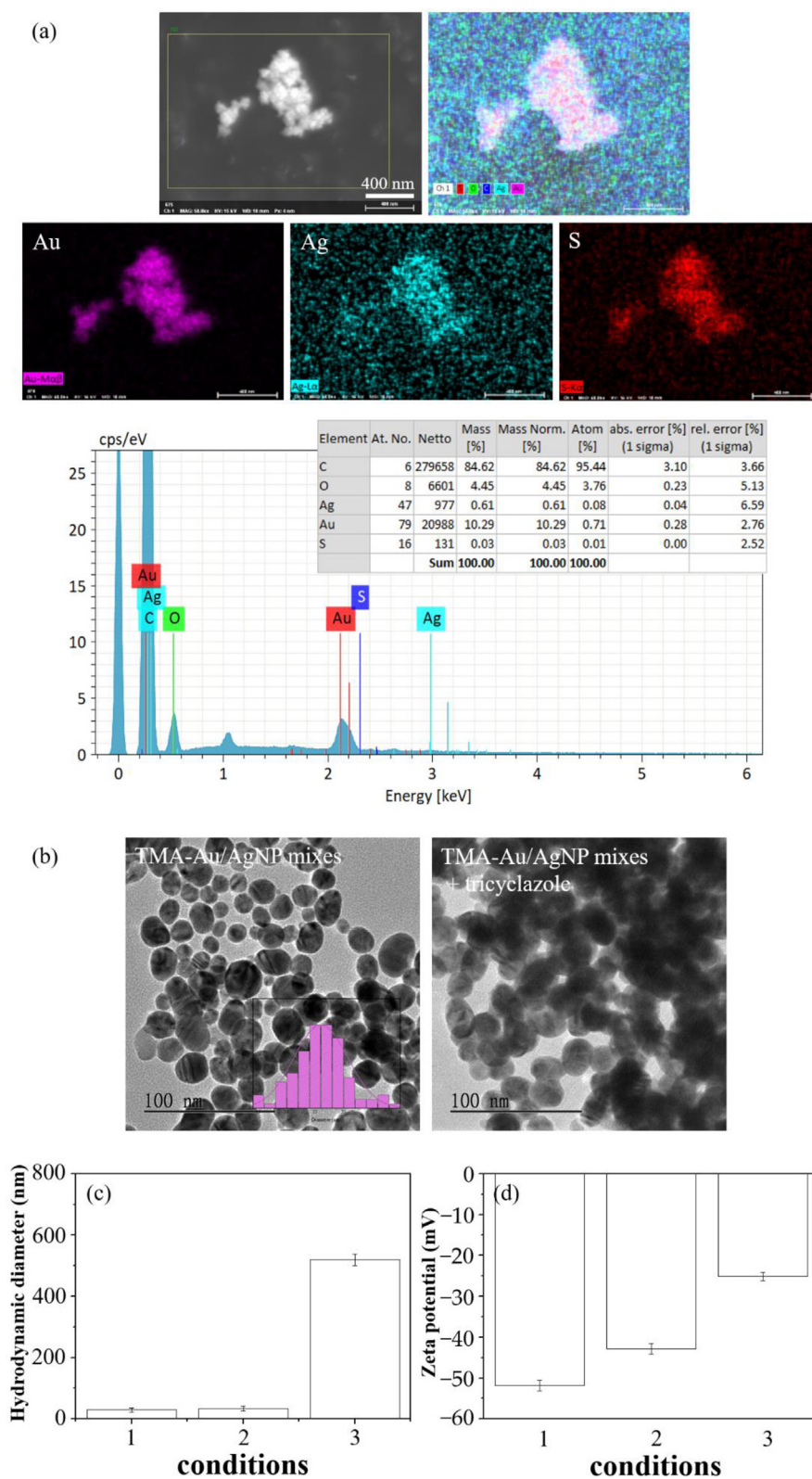
Fig. 1. (a) SEM images, EDS mapping and EDS spectrum of TMA-Au/AgNP mixes. (b) TEM images of TMA-Au/AgNP mixes in the absence and the presence of tricyclazole (0.3 ppm). (c) Hydrodynamic diameter and (d) zeta potential of (1) bare Au/AgNP mixes, TMA-Au/AgNP mixes in (2) the absence and (3) the presence of tricyclazole (0.3 ppm).

owing to structural similarities with triazole-group pesticides, it can be considered a triazole-group pesticide. In this study, we used TMA-Au/AgNP mixes as colorimetric probes to detect tricyclazole in the presence of 10 mM Tris−HCl buffer at pH 7.0. The UV−Vis spectra and photographic pictures of the TMA-Au/AgNP mixes solutions in the absence and presence of tricyclazole (0.3 ppm) are displayed in Fig. 2a. Notably, with the addition of tricyclazole, the color of the TMA-Au/AgNP mixes changed from orange-red to lavender (inset in Fig. 2a). Furthermore, tricyclazole caused the aggregation of the TMA-Au/AgNP mixes. Therefore, the distinctive SPR peaks of TMA-Au/AgNP mixes at 520 nm shifted to 654 nm. Fig. 2b displays the FT-IR spectra of tricyclazole and TMA-Au/AgNP mixes with tricyclazole. The tricyclazole spectrum (black in Fig. 2b) displays distinctive peaks corresponding to C=N vibration at 1496 cm^{-1}, C−N stretching vibrations at 1217, 1148, and 1044 cm^{-1}, and C−S stretching vibrations at 786, 723, and 647 cm^{-1}. Upon the addition of tricyclazole to TMA-Au/AgNP mixes, the peaks attributable to the C=N, C−N, and C−S moieties of pure tricyclazole occurred at similar wavenumbers (red in Fig. 2b). Fig. 2c illustrates the Raman spectra of tricyclazole and TMA-Au/AgNP mixes with tricyclazole. The spectrum (black in Fig. 2c) displays distinctive peaks corresponding to C−N−C vibrations at 421 cm^{-1}, C−S−C vibrations at 590 cm^{-1}, C=C vibrations at 971 cm^{-1}, and C−N stretching vibrations at 1315 and 1364 cm^{-1}. Upon the addition of tricyclazole to TMA-Au/AgNP mixes, peaks assigned to pure tricyclazole moieties were observed at similar chemical shifts (red in Fig. 2c). Therefore, these tricyclazole functional groups may have interacted with the TMA-Au/AgNP mixes. This was further verified by the results of TEM and DLS. The TEM images and DLS (hydrodynamic diameter and zeta potential) of the TMA-Au/AgNP mixes with tricyclazole are displayed in Fig. 1b, c, and 1d. Because of the aggregation induced by tricyclazole, the hydrodynamic diameter of the TMA-Au/AgNP mixes increased to 519 ± 9 nm (Fig. 1c). In addition, upon the addition of tricyclazole, the zeta potential decreased to −25.1 ± 1.1 mV. The interactions between tricyclazole and TMA-Au/AgNP mixes were further indicated by these data. These findings strongly suggested that tricyclazole caused the TMA-Au/AgNP mixes aggregation.

3.4. Optimum conditions

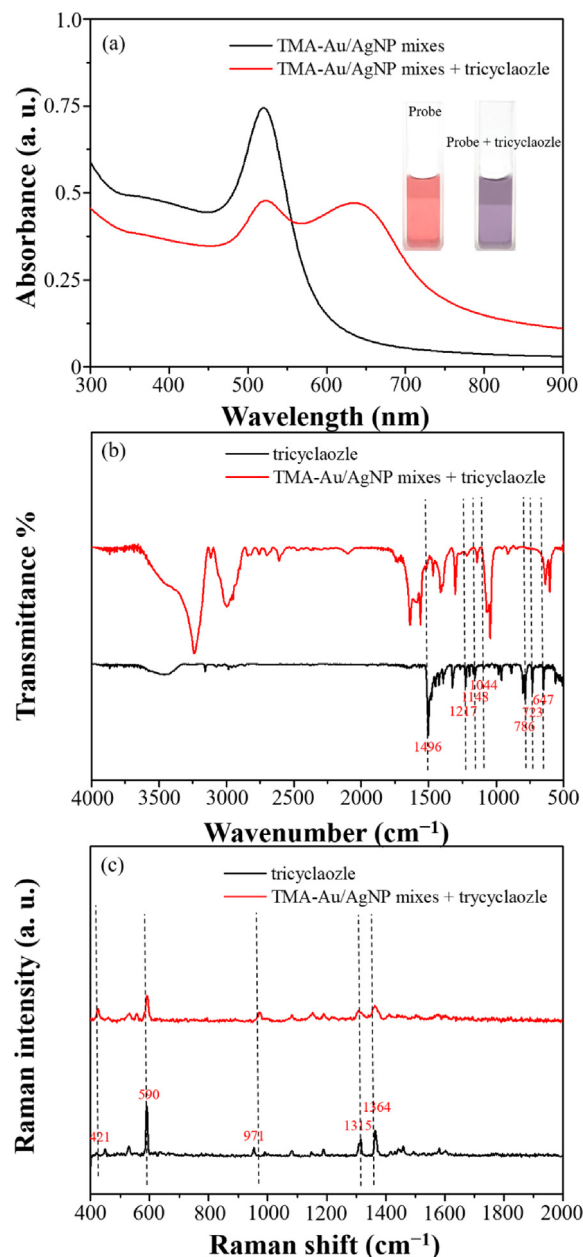The pH, Tris−HCl concentration, and TMA concentration for the sensing conditions were

Fig. 2. (a) UV−Vis spectra of TMA-Au/AgNP mixes in the absence and presence of tricyclazole (0.3 ppm) in Tri-HCl buffer (pH 7.0, 10 mM). Inset: Photograph of TMA-Au/AgNP mixes in the absence and presence of tricyclazole. (b) FT-IR and (c) Raman spectra of tricyclazole and TMA-Au/AgNP mixes in the presence of tricyclazole (0.3 ppm).

subsequently optimized for the colorimetric assay. The sensing ability of TMA-Au/AgNP mixes in the absence ($R_0 = A_{654}/A_{520}$) and presence ($R = A_{654}/A_{520}$) of tricyclazole was assessed according to the ratio change ((R_0 − R)/R_0). As illustrated in Fig. 3a−c, changing the pH (5.0−9.0), Tris−HCl concentration (0.001−10.0 mM), and TMA concentration (0.01−1.0 mM) had no observable influence on the colorimetric detection of tricyclazole. Thus, the parameters for the following experimental
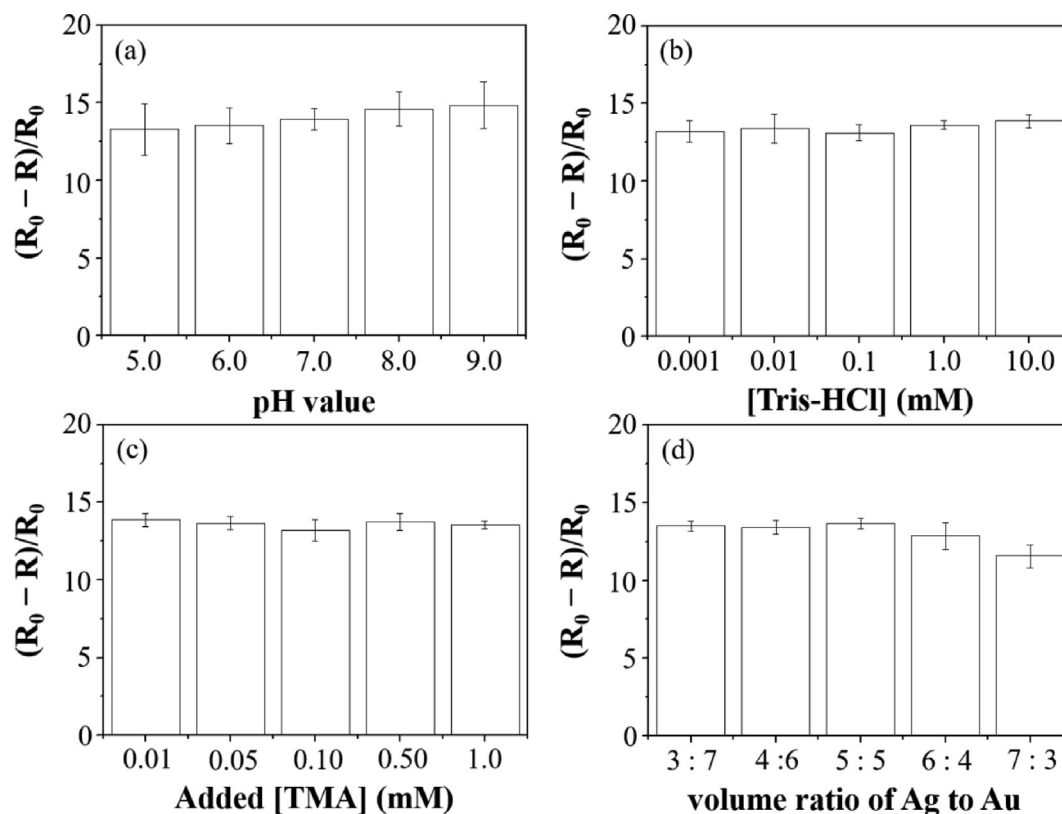
Fig. 3. Optimum evaluation of the colorimetric detection of tricyclazole (0.5 ppm) by using TMA-Au/AgNP mixes probe: (a) pH values, (b) Tris−HCl concentration, (c) TMA concentration, and (d) volume ratios of TMA-AuNPs to TMA-AgNPs.

analysis were selected as follows: pH 7.0, 10 mM Tris−HCl, and 0.01 mM TMA concentration. The volume ratios of the TMA-AgNPs to TMA-AuNPs influenced the interactions between TMA-Au/AgNP mixes and tricyclazole. Therefore, the ratio $(R_0 - R)/R_0$ of TMA-Au/AgNP mixes in the presence and absence of tricyclazole were measured (Fig. 3d). The ratio $(R_0 - R)/R_0$ of TMA-Au/AgNP mixes almost remained constant when the volume ratio of TMA-AgNPs to TMA-AuNPs was increased from 3:7 to 5:5. However, when the volume ratio was increased to 6:4, the ratio $(R_0 - R)/R_0$ slightly decreased. This is due to the fact that the interaction strength of TMA-AuNPs with tricyclazole was greater than that of TMA-AgNPs with tricyclazole. We later used density-functional theory calculations to prove this assumption. Thus, a volume ratio of TMA-AgNPs to TMA-AuNPs at 5:5 was selected for the colorimetric detection of tricyclazole.

3.5. Sensing mechanism of TMA-Au/AgNP mixes toward tricyclazole

As the donor for tricyclazole sensing, the TMA molecules on the AgNPs and AgNPs surface are crucial. According to density-functional theory (DFT) calculations, the electron-rich carbonic group of TMA on the AgNPs and AgNPs surface interacts strongly with the electron-poor aromatic ring of tricyclazole (Fig. S3 [https://www.jfda-online.com/cgi/viewcontent.cgi?filename=0&article=3450&context=journal&type=additional]). Tricyclazole adsorbed on TMA/Au (111) and TMA/Ag (111) surfaces with the adsorption energies of −0.52 eV and −0.48 eV, respectively. The net atomic charge calculation by using Bader's method shows that the tricyclazole obtained 0.06 and 0.04 electrons after adsorption for the TMA/Au (111) and TMA/Ag (111) surfaces, respectively, as shown in Fig. S4 [https://www.jfda-online.com/cgi/viewcontent.cgi?filename=0&article=3450&context=journal&type=additional]. These findings indicated that the interaction strength between TMA-AuNPs and tricyclazole was greater than that between TMA-AgNPs and tricyclazole. Thus, the electron donor−acceptor interaction between tricyclazole and TMA causes the TMA-Au/AgNP mixes to aggregate as shown in Scheme 1. Tricyclazole was consequently added, and the intensity of the characteristic SPR peak (520 nm) decreased drastically. Further, a new and
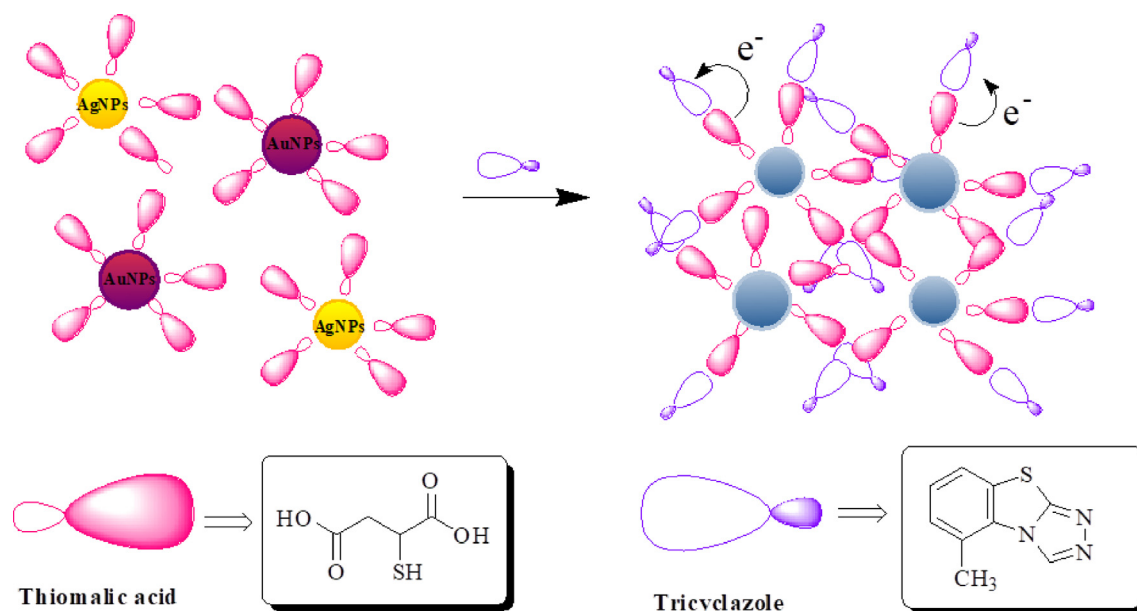
Scheme 1. Schematic of the colorimetric detection of tricyclazole using TMA-Au/AgNP mixes.

strong absorbance peak was observed at 654 nm, which was confirmed by both UV−Vis spectrometry and visual inspection.

3.6. Sensitivity and selectivity

Various concentrations of tricyclazole were added to the TMA-Au/AgNP mixes in 10 mM Tris−HCl buffer at pH 7.0 under optimum conditions, and the measured UV−Vis spectra and photographs are displayed in Fig. 4a. The color of the solutions gradually changed from orange-red to lavender as the concentration of tricyclazole increased. Furthermore, when the concentration of tricyclazole was increased, the intensity of the SPR peak of the TMA-Au/AgNP mixes at 520 nm gradually decreased, and a new peak was observed at 654 nm. These results indicated that the level of aggregation in the TMA-Au/AgNP mixes can increase with increasing tricyclazole concentration. As illustrated in Fig. 4b, the absorbance ratio (A_{654}/A_{520}) increases with the increasing concentration of tricyclazole. The absorbance ratios (A_{654}/A_{520}) were linearly related to the concentration of tricyclazole, which ranged from 0.1 to 0.5 ppm. The linear relation was obtained using the regression equation $y = 0.054 + 1.81x$ ($R^2 = 0.948$). The LOD was 0.028 ppm. The absorption spectra of the bare Au/AgNP mixes after the addition of tricyclazole of various concentrations under the same conditions are displayed in Fig. S5 [https://www.jfda-online.com/cgi/viewcontent.cgi?filename=0&article=3450&context=journal&type=additional]. Due to the lack of charge transfer between tricyclazole and TMA, the concentration ranges between 0.1 and 0.5 ppm are nonlinear (Inset in Fig. S5 [https://www.jfda-online.com/cgi/viewcontent.cgi?filename=0&article=3450&context=journal&type=additional]).

To detect tricyclazole, TMA functionalized Au/AgNP mixes could act as colorimetric probes rather than bare Au/AgNP mixes. Furthermore, Figs. S6a and S6b [https://www.jfda-online.com/cgi/viewcontent.cgi?filename=0&article=3450&context=journal&type=additional] show the absorption spectra of pure TMA-AgNPs and pure TMA-AuNPs after the addition of various concentrations of tricyclazole, respectively. Both concentration ranges from 0.1 to 0.5 ppm are nonlinear due to the particle size and concentration effects (Inset in Figs. S6a and S6b [https://www.jfda-online.com/cgi/viewcontent.cgi?filename=0&article=3450&context=journal&type=additional]). As a sensing probe, TMA-AgNPs coupled with TMA-AgNPs are necessary for improved tricyclazole sensing linearity and sensitivity [40,41]. Moreover, utilizing TMA-Au/AgNP mixes can decrease the cost of determination comparing to pure TMA-AuNPs.

In comparison to earlier colorimetric studies, our proposed method had advantages such as fast synthesis of TMA-Au/AgNPs, short sample pretreatment time, high selectivity, and a similar LOD [29,30]. However, a low LOD for tricyclazole determination was calculated using a surface-enhanced Raman scattering (SERS) technique [27,28,42,43]. Thus, we
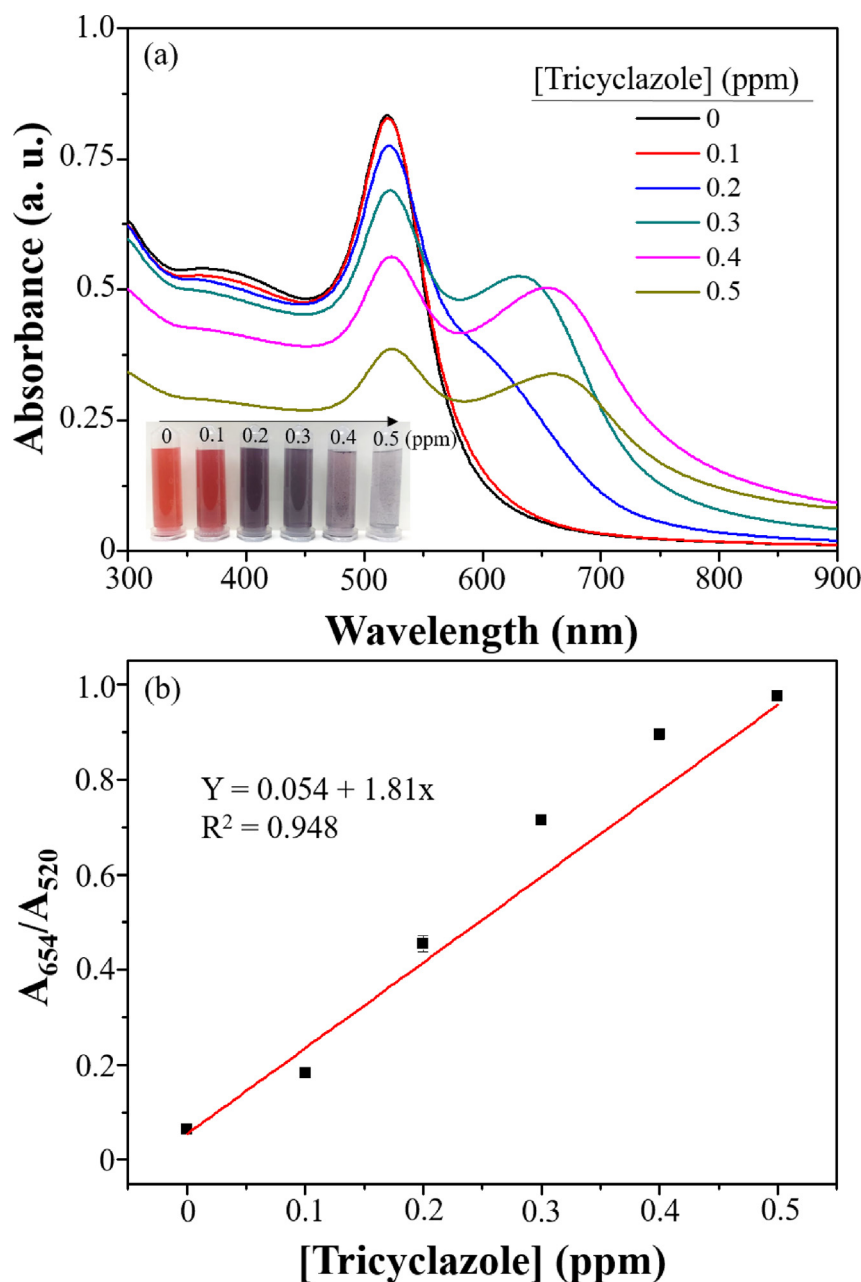
Fig. 4. (a) UV–Vis spectra of TMA-Au/AgNP mixes with the increasing concentration of tricyclazole from 0 to 0.5 ppm. Inset: Photograph of TMA-Au/AgNP mixes solution with the increasing concentration of tricyclazole from 0 to 0.5 ppm. (b) Calibration graph between the absorbance ratio of A_{654}/A_{520} and the different concentrations of tricyclazole from 0 to 0.5 ppm.

are currently developing TMA-Au/AgNPs mixes that will be deposited on a SERS-active Au(Ag) substrate for enhanced tricyclazole sensitivity [44–51].

We measured the UV–Vis absorption responses for a variety of pesticides, including carbendazim, dimethoate, trichlorfon, dichlorves, chlorothalonil, chlorpyrifos, clothianidin, glufosinate-ammonium, methomyl, 2,4-D, propanil, glyphosate, dicofol, carbaryl, fenvalerate, thiodicarb, acetamiprid, kresoxim-methyl, cartap, carbofuran, pencycuron, profenofos, imidacloprid, bifenthrin, and tricyclazole. The investigation revealed that, with the exception of tricyclazole, the majority of pesticides had little to no effect on the color of TMA-Au/AgNP mixes solution. All examined vials displayed an orange-red color; however, only tricyclazole caused a color change in TMA-Au/AgNP mixes, as illustrated in photographs of Fig. 5a. Thus, the colorimetric assay was very selective for tricyclazole. Additionally, as shown in Fig. S7 [https://www.jfda-online.
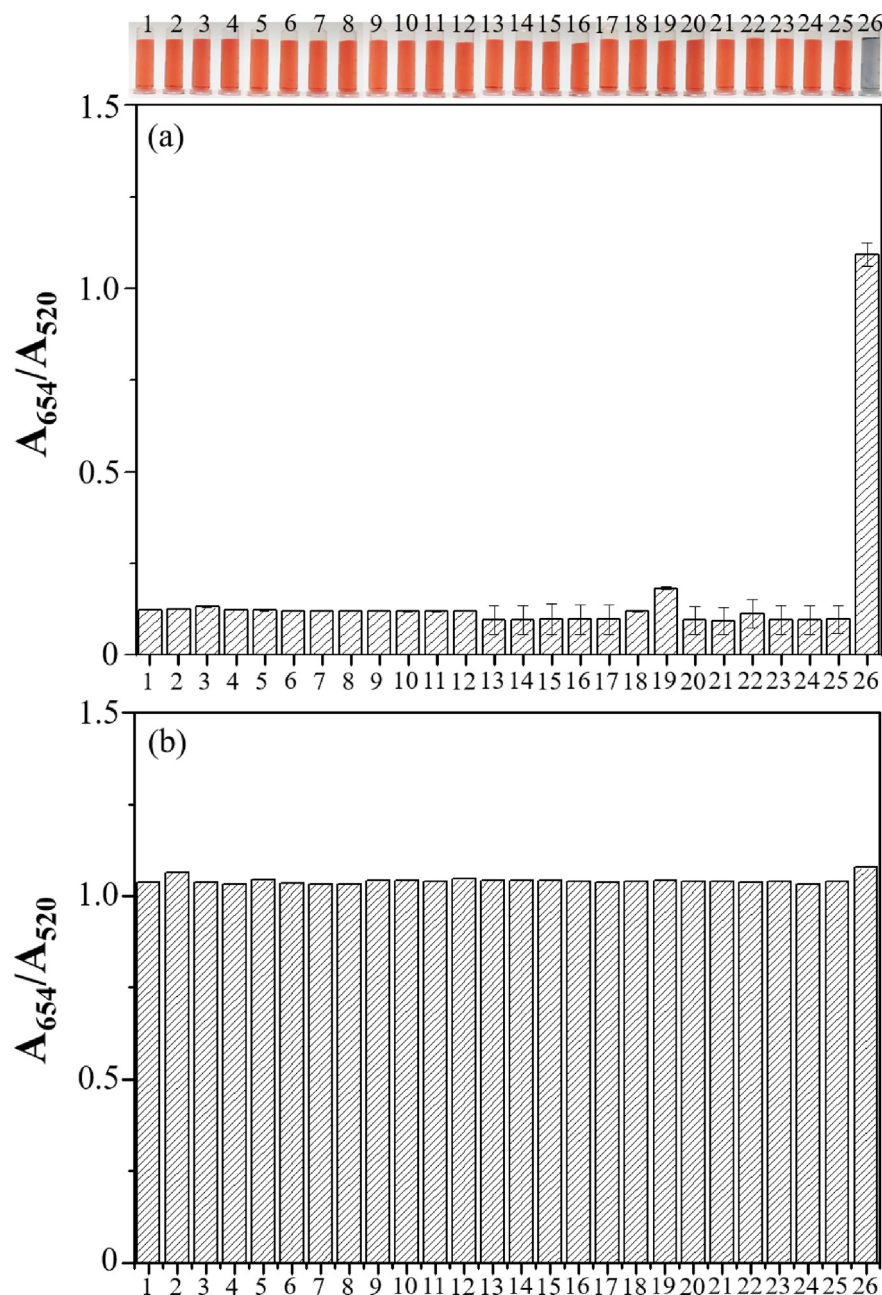
Fig. 5. (a) Selectivity of (1) TMA-Au/AgNP mixes with (2) carbendazim, (3) dimethoate, (4) trichlorfon, (5) dichlorves, (6) chlorothalonil, (7) chlorpyrifos, (8) clothianidin, (9) glufosinate-ammonium, (10) methomyl, (11) 2,4-D, (12) propanil, (13) glyphosate, (14) dicofol, (15) carbaryl, (16) fenvalerate, (17) thiodicarb, (18) acetamiprid, (19) kresoxim-methyl, (20) cartap, (21) carbofuran, (22) pencycuron, (23) profenofos, (24) imidacloprid, (25) bifenthrin, and (26) tricyclazole (each pesticide: 0.5 ppm). Photographs displaying the color variations of TMA-Au/AgNP mixes solutions in the (1) absence and presence of (2—26) different pesticides. (b) Tolerance of TMA-Au/AgNP mixes in the presence of (1) tricylazeole (0.5 ppm) and (2—26) different pesticides (5.0 ppm).

the absorbance ratios of TMA-AgNPs (A_{733}/A_{390}) and TMA-AuNPs (A_{654}/A_{520}) were calculated for selective test. Reduced selectivity was observed in both cases; for instance, TMA-AgNPs aggregation was induced by kresoxim-methyl and carbofuran. Carbendazim, kresozim-methyl, pencycuron, and profenofos caused TMA-AuNPs to aggregate. In comparison to pure TMA-AgNPs and pure TMA-AuNPs, we assumed that in the case of TMA-Au/AgNP mixes, the appropriate adsorption energy for the interaction between TMA and tricyclazole was achieved, resulting in higher selectivity toward tricyclazole.

Table 1. Detection of tricyclazole in tap water, apple juice, and rice samples (n = 3).

Sample	Added (ppm)	Found (ppm)	Recovery (%)	RSD (%)
Tap water	0.200	0.195	97.5	2.8
	0.300	0.285	95.0	2.3
	0.400	0.411	102.8	2.4
Apple juice	0.200	0.198	99.0	2.8
	0.300	0.293	97.7	2.7
	0.400	0.421	105.2	2.5
Rice	0.200	0.197	98.5	2.8
	0.300	0.301	100.3	2.3
	0.400	0.398	99.5	2.4

Further DFT calculations to prove our hypothesis is now underway in our laboratory. We then calculated the absorbance ratio (A_{654}/A_{520}) of TMA-Au/AgNP mixes in the presence of coexisting pesticides (5.0 ppm) and 0.5 ppm tricyclazole. The analysis revealed that interferences did not influence the aggregation of TMA-Au/AgNP mixes (Fig. 5b). Thus, TMA-Au/AgNP mixes exhibited a high level of tolerance for tricyclazole.

3.7. Applications

To confirm the potential applicability and accuracy of the proposed colorimetric assay, tap water, apple juice, and rice samples were spiked with known concentrations of tricyclazole. As displayed in Table 1, with relative standard deviations (RSDs) less than 2.8%, good recoveries were observed in the tap water (97.5%—102.8%), apple juice (97.7%—105.2%), and rice (98.5%—100.3%) samples. Therefore, the proposed colorimetric assay can be utilized to detect tricyclazole in real samples.

When compared to previous nanoparticle-based probes (Table 2), this one-of-a-kind TMA-Au/AgNP mixes has several compelling characteristics: (1) simplicity and convenience of use—no complicated

sample preparation and instrument operation are necessary; (2) good stability, selectivity, and sensitive performance—the LOD for the determination of tricyclazole was 0.028 ppm—and (3) applicability—tricyclazole was determined in tap water, apple juice, and rice samples [27—30,42,43]. This study not only provides a complete examination of the electron exchange between TMA and tricyclazole, but it also provides evidence for their practical application potential.

4. Conclusions

We proposed a colorimetric assay for the detection of tricyclazole by using TMA-Au/AgNPs mixes. When tricyclazole was added, the color of the solution changed from orange-red to lavender, and the SPR band of TMA-Au/AgNPs mixes exhibited an obvious red shift (λ_{max}: 520—654 nm). According to the density-functional theory calculations, the electron donating and accepting interaction between TMA and tricyclazole causes the sensing mechanism of this colorimetric probe. The linear range for determination of tricyclazole was 0.1—0.5 ppm ($R^2 = 0.948$) with a LOD of 0.028 ppm, which is below the maximum residue limits stipulated by the European Union and Taiwan (0.1 and 3.0 ppm, respectively). In comparison to bare Au/AgNPs mixes, pure TMA-AuNPs, and pure TMA-AuNPs probes, the proposed TMA-Au/AgNPs mixes provided higher selectivity and sensitivity due to appropriate size, concentration, and charge transition parameters. The spiked recoveries of tricyclazole in tap water, apple juice, and rice samples were 97.5%—102.8%, 97.7%—105.2%, and 98.5%—100.3% respectively. Thus, the proposed approach has the advantages of ease of operation, simplicity, selectivity, and reproducibility for determining tricyclazole in real samples.

Table 2. Nanoparticle-based optical method for the determination of trycyclazole.

Method	Probe	Analytical range (ppm)	LOD (ppm)	Real sample	Ref.
Surface enhanced Raman scattering	AgNPs + pryidine	0.05—0.7	0.02	Rice	[42]
	AuNRs	0.02—2.0	0.02	Apple peel	[43]
	AuNPs	0.5—10	0.50	Rice	[28]
	MCO/Au@AgNPs	0.05—5	0.004	Pear	[27]
Colorimetric	SADTC-AgNPs	0.189—18.9	0.034	Rice	[29]
	F-AgNPs	0.06—1.0	0.051	Rice	[30]
	TMA-Au/AgNP mixes	0.1—0.5	0.028	Tap water, apple juice, rice	This study

Declaration of competing interest

There are no conflicts to declare.

Acknowledgements

References

[1] Li C, Chen Y, Huang L, Zhang Y, Cao N, Guo X, et al. Potential toxicity and dietary risk of tricyclazole to Chinese mitten crab (Eriocheir sinensis) in the rice-crab co-culture model. Environ Pollut 2023;316:120514.

[2] Laskar N, Ghoshal D, Gupta S. Molecularly imprinted polymers for selective sorption of tricyclazole in food. ChemistrySelect 2022;7:e202201019.

[3] Wei Y, Shen X, Zhang L, Tang J, Xu T, Xu M, et al. PDMS-based SERS substrate of high sensitivity and uniformity and its application in in situ detection of tricyclazole. Nano 2022:2250034.

[4] Nguyen DN, Nguyen HT, Pham T-L, Nguyen CT, Duong HTG, Nguyen HQ, et al. Degradation of tricyclazole from aqueous solution and real wastewater by electron-beam irradiation. Environ Technol Innovat 2021;21:101315.

[5] Corvaro M, Bartels M. The ADME profile of the fungicide tricyclazole in rodent via the oral route: a critical review for human health safety assessment. Regul Toxicol Pharmacol 2019;108:104438.

[6] Padovani L, Capri E, Padovani C, Puglisi E, Trevisan M. Monitoring tricyclazole residues in rice paddy watersheds. Chemosphere 2006;62:303−14.

[7] Wu H, Zhao J, Yang XN, Yang D, Chen LX, Redshaw C, et al. A cucurbit [8] uril-based probe for the detection of the pesticide tricyclazole. Dyes Pigments 2022;199:110076.

[8] Nguyen CT, Vo TT, Nguyen TX, Nguyen HP, Bui DD, Nguyen VM, et al. Assessment of pesticide residues in organic rice production in the Mekong Delta, Vietnam. Eur J Develop Stud 2022;2:1−11.

[9] WHO G. The WHO recommended classification of pesticides by hazard and guidelines to classification 2009. 2010.

[10] Romniou SE, Nana K, Dasenaki M, Komaitis E, Proestos C. Development and validation of pesticide residues determination method in fruits and vegetables through liquid and gas chromatography tandem mass spectrometry (LC-MS/MS and GC-MS/MS) employing modified quechers method and a centrifugal vacuum concentrator. Agriculture-Basel 2022;12:1936.

[11] Na TW, Seo H-J, Jang S-N, Kim H, Yun H, Kim H, et al. Multi-residue analytical method for detecting pesticides, veterinary drugs, and mycotoxins in feed using liquid-and gas chromatography coupled with mass spectrometry. J Chromatogr A 2022;1676:463257.

[12] Wang H, Ping H, Liu Q, Han P, Guo X. Determination of pesticide residues in strawberries by ultra-performance liquid chromatography-tandem mass spectrometry. Food Anal Methods 2022;15:85−95.

[13] Bao S. Evaluation on uncertainty for the contents of tricyclazole in 75%WP by HPLC. Mod Agrochem 2009;8:28−30.

[14] Tsochatzis ED, Menkissoglu-Spiroudi U, Karpouzas DG, Tzimou-Tsitouridou R. A multi-residue method for pesticide residue analysis in rice grains using matrix solid-phase dispersion extraction and high-performance liquid chromatography−diode array detection. Anal Bioanal Chem 2010;397:2181−90.

[15] Phong TK, Nhung DTT, Yamazaki K, Takagi K, Watanabe H. Behavior of sprayed tricyclazole in rice paddy lysimeters. Chemosphere 2009;74:1085−9.

[16] Wang J, Xu J, Ji X, Wu H, Yang H, Zhang H, et al. Determination of veterinary drug/pesticide residues in livestock and poultry excrement using selective accelerated solvent extraction and magnetic material purification combined with ultra-high-performance liquid chromatography−tandem mass spectrometry. J Chromatogr A 2020;1617:460808.

[17] Naik RH, Pallavi M, Kumar P, Nidoni UK, Bheemanna M, Paramasivam M. Determination of tricyclazole fungicide in rice using LC-MS/MS and its risk assessment. Pestic Res J 2020;32:148−58.

[18] Lee SJ, Park HJ, Kim W, Jin JS, Abd El Aty A, Shim JH, et al. Multiresidue analysis of 47 pesticides in cooked wheat flour and polished rice by liquid chromatography with tandem mass spectrometry. Biomed Chromatogr 2009;23:434−42.

[19] Pareja L, Colazzo M, Perez-Parada As, Besil N, Heinzen H, Bocking B, et al. Occurrence and distribution study of residues from pesticides applied under controlled conditions in the field during rice processing. J Agric Food Chem 2012;60:4440−8.

[20] Xu X, Wang S, Hou S, Li Z, Lu Z, Liang S. A multi-residue method for the determination of 77 pesticides in red ginseng using quechers and gas chromatography/tandem mass spectrometry (GC-MS/MS). Agronomy-Basel 2022;12:2479.

[21] Pengyan L, Qingxue L, Yusong M, Jinwei L, Xuan J. Analysis of pesticide multiresidues in rice by gas chromatography-mass spectrometry coupled with solid phase extraction. Chin J Chromatogr 2006;24:228−34.

[22] Wang Y, Jin H-Y, Ma S-C, Lu J, Lin R-C. Determination of 195 pesticide residues in Chinese herbs by gas chromatography−mass spectrometry using analyte protectants. J Chromatogr A 2011;1218:334−42.

[23] Wei S-C, Lin Y-W, Chang H-T. Carbon dots as artificial peroxidases for analytical applications. J Food Drug Anal 2020;28.

[24] Lin Y-W, Huang C-C, Chang H-T. Gold nanoparticle probes for the detection of mercury, lead and copper ions. Analyst 2011;136:863−71.

[25] Lin Y-W, Liu C-W, Chang H-T. DNA functionalized gold nanoparticles for bioanalysis. Anal Methods 2009;1:14−24.

[26] Chu H-W, Unnikrishnan B, Anand A, Lin Y-W, Huang C-C. Carbon quantum dots for the detection of antibiotics and pesticides. J Food Drug Anal 2020;28.

[27] Hussain N, Pu H, Sun D-W. Core size optimized silver coated gold nanoparticles for rapid screening of tricyclazole and thiram residues in pear extracts using SERS. Food Chem 2021;350:129025.

[28] Zhang W, Liu Z, Qin H, Li H, Du H, Fang L, et al. Surface-enhanced Raman spectroscopy coupled with dispersive solid phase extraction for the rapid detection of tricyclazole residues in rice and Brassica campestris L. ssp. chinensis var. utilis Tsen. Anal Sci 2020:20P166.

[29] Rohit JV, Kailasa SK. 5-sulfo anthranilic acid dithiocarbamate functionalized silver nanoparticles as a colorimetric probe for the simple and selective detection of tricyclazole fungicide in rice samples. Anal Methods 2014;6:5934−41.

[30] Su Y-C, Lin A-Y, Hu C-C, Chiu T-C. Functionalized silver nanoparticles as colorimetric probes for sensing tricyclazole. Food Chem 2021;347:129044.

[31] Kresse G, Furthmuller J. Efficiency of ab-initio total energy calculations for metals and semiconductors using a plane-wave basis set. Comput Mater Sci 1996;6:15−50.

[32] Kresse G, Furthmuller J. Efficient iterative schemes for ab initio total-energy calculations using a plane-wave basis set. Phys Rev B 1996;54:11169.

[33] Perdew JP, Burke K, Ernzerhof M. Generalized gradient approximation made simple. Phys Rev Lett 1996;77:3865.

[34] Kresse G, Joubert D. From ultrasoft pseudopotentials to the projector augmented-wave method. Phys Rev B 1999;59:1758.

[35] Grimme S, Antony J, Ehrlich S, Krieg H. A consistent and accurate ab initio parametrization of density functional dispersion correction (DFT-D) for the 94 elements h-pu. J Chem Phys 2010;132:154104.

[36] Grimme S, Ehrlich S, Goerigk L. Effect of the damping function in dispersion corrected density functional theory. J Comput Chem 2011;32:1456−65.

[37] Davey WP. Precision measurements of the lattice constants of twelve common metals. Phys Rev 1925;25:753.

[38] Jette ER, Foote F. Precision determination of lattice constants. J Chem Phys 1935;3:605−16.

[39] Tang W, Sanville E, Henkelman G. A grid-based Bader analysis algorithm without lattice bias. J Phys Cond Matter 2009;21:084204.

[40] Thongkam T, Apilux A, Tusai T, Parnklang T, Kladsomboon S. Thy-AuNP-AgNP hybrid systems for colorimetric determination of copper (II) ions using UV-Vis spectroscopy and smartphone-based detection. Nanomaterials 2022;12:1449.

[41] Sahu S, Sharma S, Ghosh KK. Novel formation of Au/Ag bimetallic nanoparticles from a mixture of monometallic nanoparticles and their application for the rapid detection of lead in onion samples. New J Chem 2020;44:15010−7.

[42] Tang H, Fang D, Li Q, Cao P, Geng J, Sui T, et al. Determination of tricyclazole content in paddy rice by surface enhanced Raman spectroscopy. J Food Sci 2012;77:T105−9.

[43] Kwon G, Kim J, Kim D, Ko Y, Yamauchi Y, You J. Nanoporous cellulose paper-based SERS platform for multiplex detection of hazardous pesticides. Cellulose 2019;26:4935−44.

[44] Lin Y-W, Tang C. Electrochemical synthesis and deposition of surface-enhanced Raman scattering-active silver microstructures on a screen-printed carbon electrode. J Phys Chem C 2015;119:24865−74.

[45] You Y-H, Lin Y-W, Chen C-Y. Surface-enhanced Raman scattering-active desert-rose-like Ag mesoparticles prepared using cyclic voltammetric methods. RSC Adv 2015;5:93293−300.

[46] Wu T, Lin Y-W. Surface-enhanced Raman scattering active gold nanoparticle/nanohole arrays fabricated through electron beam lithography. App Sur Sci 2018;435:1143−9.

[47] Chen J-L, Wu T, Lin Y-W. Surface-enhanced Raman scattering enhancement due to localized surface plasmon resonance coupling between metallic nanoparticles and substrate. Microchem J 2018;138:340−7.

[48] Chen J-L, Yang P-C, Wu T, Lin Y-W. Determination of mercury (II) ions based on silver-nanoparticles-assisted growth of gold nanostructures: UV−Vis and surface enhanced Raman scattering approaches. Spectroc Acta Pt A-Molec Biomolec Spectr 2018;199:301−7.

[49] Yang P-C, Lin P-H, Huang C-C, Wu T, Lin Y-W. Determination of Hg (II) based on the inhibited catalytic growth of surface-enhanced Raman scattering-active gold nanoparticles on a patterned hydrophobic paper substrate. Microchem J 2020;157:104983.

[50] Huang HJ, Shiao M-H, Lin Y-W, Lin B-J, Su J, Lin Y-S, et al. Au@Ag dendritic nanoforests for surface-enhanced Raman scattering sensing. Nanomaterials 2021;11:1736.

[51] Shiao M-H, Wu T, Huang HJ, Peng C-Y, Lin Y-S, Lai T-Y, et al. Dendritic forest-like Ag nanostructures prepared using fluoride-assisted galvanic replacement reaction for SERS applications. Nanomaterials 2021;11:1359.